ADVANCES IN ATMOSPHERIC SCIENCES, VOL. 22, NO. 6, 2005, 903–914

Resolving SSM/I-Ship Radar Rainfall Discrepancies from AIP-3

Song YANG*[1] and Eric A. SMITH[2]

[1]*School of Computational Sciences, George Mason University, Fairfax, VA, USA*

[2]*NASA/Goddard Space Flight Center, Greenbelt, MD, USA*

(Received 25 February 2005; revised 9 June 2005)

ABSTRACT

The third algorithm intercomparison project (AIP-3) involved rain estimates from more than 50 satellite rainfall algorithms and ground radar measurements within the Intensive Flux Array (IFA) over the equatorial western Pacific warm pool region during the Tropical Ocean Global Atmosphere coupled Ocean-Atmosphere Response Experiment (TOGA COARE). Early results indicated that there was a systematic bias between rainrates from satellite passive microwave and ground radar measurements. The mean rainrate from radar measurements is about 50% underestimated compared to that from passive microwave-based retrieval algorithms. This paper is designed to analyze rain patterns from the Florida State University rain retrieval algorithm and radar measurements to understand physically the rain discrepancies. Results show that there is a clear range-dependent bias associated with the radar measurements. However, this range-dependent systematical bias is almost eliminated with the corrected radar rainrates. Results suggest that the effects from radar attenuation correction, calibration and beam filling are the major sources of rain discrepancies. This study demonstrates that rain retrievals based on satellite measurements from passive microwave radiometers such as the Special Sensor of Microwave Imager (SSM/I) are reliable, while rain estimates from ground radar measurements are correctable.

Key words: rainfall, SSM/I, radar, satellite microwave measurements

1. Introduction

Satellite remote sensing is considered to be the best way to obtain precipitation and other meteorological variables over tropical oceans because of the lack of conventional meteorological networks and off-coast radar information and the great expense of aircraft operations. Visible and infrared (VIS/IR) satellite observations have been used to estimate rainfall by different investigators (e.g., Arkin, 1979; Adler and Negri, 1988; Atlas et al., 1990). Since clouds tend to be opaque to VIS/IR radiation, rainfall from VIS/IR must be inferred indirectly, and the relationship between rainrate and VIS/IR brightness temperature is purely empirical. Therefore, VIS/IR or IR-only rainrate retrieval algorithms must be carefully calibrated using surface rainfall observations. Any relation between rainrate and VIS/IR applied at a given region might not be suitable for other areas.

Since microwave radiation has the ability to penetrate clouds and directly sense precipitation particles, rainrate retrievals using satellite measurements in the microwave regime have been investigated for several decades. Wilheit et al. (1977) first demonstrated oceanic rainfall retrievals utilizing 19-GHz measurements from the Nimbus-5 ESMR. Many statistical and physical algorithms have since been developed, including single- and multi-frequency-based algorithms. The applications of multi-frequency channels, especially the scattering channels of passive microwave radiometers, in the physical inversion profiling rain algorithms have dramatically improved the accuracy of rainfall retrievals. For example, Spencer et al. (1989) applied a polarized corrected temperature (PCT) scheme with SSM/I measurements to retrieve rainfall. Kummerow et al. (1989, 1991) developed an inversion algorithm that produces complete rainrate profiles based on microphysical structures generated from aircraft radar data. Hinton et al. (1992) combined a group of single-channel brightness temperature rainrate relationships into a multichannel algorithm using a hybrid physical-statistical method for rainfall retrievals. Adler et al. (1993) applied both the physically-based microwave retrievals and rainrates from IR measurements based

*E-mail: ysong@agnes.gsfc.nasa.gov

on the Geostationary Operational Satellite Precipitation Index (GPI; Arkin and Meisner, 1987). This method takes advantage of the better IR sampling and rain accuracy of microwave retrievals to estimate global precipitation. Smith et al. (1992, 1994a–c) and Mugnai et al. (1993) developed a physical inversion profile algorithm for retrieving vertical profiles of hydrometeors, using output from a three-dimensional nonhydrostatistic cloud model as the algorithm's initial guess information. Yang and Smith (1999a, b, 2000) improved the Florida State University (FSU) rain algorithm by introducing better estimates of surface emissivity and better databases, and they carefully analyzed its performance in surface rain retrievals and its applications in retrieving latent heating and eddy flux with combined large scale heat-moisture budgets. A review of precipitation retrievals based on satellite passive microwave measurements (PMM) by Yang (2004) provided a brief history of developments and improvements for PMM-based precipitation retrieval algorithms. The accuracy of PMM rain retrievals has been significantly improved since SSM/I data became available, especially by utilization of the PMM multi-frequency channels in physical inversion-based rain algorithms.

A fundamental problem impacting the results of past studies is the limited spatial resolution of satellite microwave measurements. The field of view (FOV) of microwave frequencies increases as frequency decreases, such that each channel effectively samples at different spatial scales. For instance, the FOVs (km×km) of SSM/I are approximately 69×43, 60×40, 37×29 and 15×13 for the 19, 22, 37, and 85 GHz channels, respectively. Such mismatches in radiometer FOV generally lead to nonlinear complications in the radiation transfer models utilized in rainrate retrieval processes (Mugnai et al., 1990). Furthermore, the spatial scales of precipitation cells are often well below the spatial scales of SSM/I ground footprints. Therefore, incomplete beam filling or nonhomogeneous beam filling will generally lead to errors in precipitation estimates to the degree that rainrate and brightness temperature (TB) have a nonlinear relationship. Smith and Kidder (1978) first pointed out that this nonlinear relationship caused a mean underestimation of rainrates for ESMR measurements. Due to the ESMR-5 single emission 19 GHz channel, its retrieved rainrates were consistently half as large as the rainrates from the Global Atlantic Tropical Experiment (GATE) radar estimates (Short and North, 1990). They indicated that the impact of incomplete beam filling in ESMR-5 measurements could explain most of the rain underestimation. A deconvolution scheme developed by Farrar and Smith (1992) could reduce the impact of the beam filling issue in rain retrievals. Although additional noise was introduced into TBs with the deconvolution scheme, an overall improvement of rain retrievals is evident (Farrar et al., 1994).

One of the most important tasks for providing evidence of reliable precipitation derived from satellite measurements is to validate the retrieved rainrates against other independent rain estimates such as from ground rain gauge and radar measurements. Another approach is to check the consistency among different satellite rain retrieval algorithms. Six algorithm intercomparison projects before the Tropical Rainfall Measuring Mission (TRMM) have been conducted, i.e., the WetNet Precipitation Intercomparison Project (PIP-1, PIP-2 and PIP-3; Barrett et al, 1994; Smith et al., 1998; Adler et al., 2001) and the Global Precipitation Climatology Project (GPCP) Algorithm Intercomparison Projects (AIP-1, AIP-2 and AIP-3; Arkin and Xie, 1994; Ebert et al., 1996; Ebert and Manton, 1998). Those projects were conducted over different environments at different spatial-temporal scales in order to demonstrate the credibility of rain estimates from satellite measurements. TRMM rain retrievals and its ground validation projects have brought satellite-based precipitation remote sensing to a higher level (Simpson et al., 1996; Kommerow et al., 2001; Haddad et al., 1997; Iguchi et al., 2000). TRMM rain products have been proved to be the most accurate precipitation estimates derived from space-borne instruments (Adler et al., 2000; Olson et al., 2005; Yang et al., 2005).

AIP-3 was conducted to evaluate satellite rain retrieval algorithms for tropical convective systems from November 1992 to February 1993 over the equatorial Western Pacific during the Tropical Ocean Global Atmosphere Coupled Ocean-Atmosphere Response Experiment (TOGA COARE). The shipboard radar rainrate observations were used as the validation data (Short et al., 1997; Ebert and Manton, 1998, Ebert et al., 1996). The vicinity of the Intensive Flux Array (IFA) during TOGA COARE and radar coverage are sketched in Fig. 1.

We will analyze the discrepancies of rain estimates from two different versions of FSU SSM/I-based rain algorithms and the versions 1 and 2 radar rainfall over the TOGA COARE IFA, discuss possible error sources, and propose and prove a hypothesis that can be applied to explain the range-dependent error distributions of rainrates from SSM/I and radar measurements. The results may shed light on current TRMM ground validation investigations and future global pre-

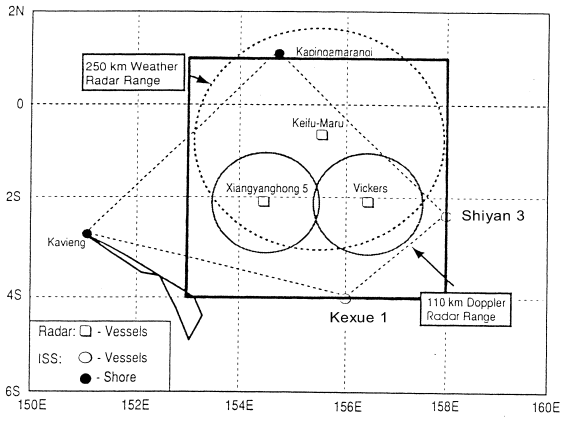

Fig. 1. The TOGA COARE Intensive Flux Array, showing locations and ranges of shipboard radars. The 5° square AIP-3 region is outlined by the bold line.

cipitation measurement (GPM) ground validation activities.

2. Methodology and dataset

Two different satellite-based rainrate datasets are applied in this study. Rainrates from satellite SSM/I measurements are based on the FSU rain retrieval algorithm. SSM/I measurements are from the Defense Satellite Meteorological Platform F10 and F11 satellites. Two different schemes have been used in processing the SSM/I data. The first scheme is the spatial deconvolution scheme (Farrar and Smith, 1992), which seeks to match FOVs of SSM/I channels before applying their TBs in rainrate retrieval processes. The deconvolution scheme is that resolutions of lower-frequency SSM/I channels are enhanced to the spatial resolution of the 85 GHz channel so that horizontal resolutions of the final rain retrievals are approximately at 15 km×13 km. Farrar et al. (1994) pointed out the impacts of the deconvolved SSM/I TBs on rain retrievals. They found that the profiling method of the rain retrieval algorithm can see the greatest improvement in retrieving instantaneous rainrates with the deconvolution scheme. The second scheme is the convolution scheme, where the resolution of the SSM/I 85 GHz channel is weighted according to the resolution of the 37 GHz channel so that the horizontal scale of the final rain retrievals is about 37 km×29 km. Therefore, two sets of rainrates from SSM/I measurements are utilized in analyzing rain discrepancies from the SSM/I and radar observations.

The radar estimates of rainrates are from two shipboard Doppler MIT and TOGA radars deployed during the intensive observation period (IOP) of TOGA CAORE (see Fig. 1). Three cruises took place during the IOP, viz.,

Cruise 1: 11/11/1992–12/10/1992
Cruise 2: 12/15/1992–01/18/1993
Cruise 3: 01/23/1993–02/23/1993

In the early stage of AIP-3, the version 1 radar rain estimates were used. Although consistent agreements exist between rain estimates from radar and other SSM/I-based retrievals, there was a serious systematic bias in which the averaged radar rainrate was about 100% underestimated. Upon considering new calibration procedures, vertical structures of the rain profiles and new $Z - R$ relationships of $Z = 120\ R^{1.43}$ for convection and $Z = 323\ R^{1.43}$ for stratiform, the version 2 radar rain estimates were generated again for the AIP-3 project. Short et al. (1997) gave a detailed description on the update of the version 2 radar rain datasets. They also suggested a range-dependent correction scheme. The overall increase of rainrates for the AIP-3 version 2 radar datasets is about 30–40% over the version 1 release. Ebert and Manton (1998) discussed the results of the AIP-3 intercomparison study in detail. The mean radar rainrate is about 50% of the averaged rainrate from SSM/I-based rain retrievals. Figure 2 shows correlation coefficients between the version 2 radar monthly rainfall and the monthly rainfall from SSM/I and general circulation model (GCM) simulations. It is evident that SSM/I-based monthly rainfall estimates have much better correlation coefficients with the radar monthly rainfall than the GCM models do. Although IR/VIS -based rain algorithms also have good correlation coefficients with radar estimates on the monthly scale, their correlations are much smaller than those from SSM/I-based rain algorithms on the instantaneous scale.

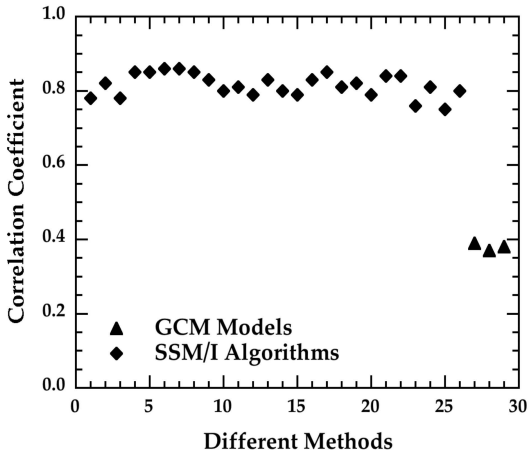

Fig. 2. Comparison of monthly surface rainfall from SSM/I algorithms and GCM models to the version 2 radar observations over the TOGA COARE IFA on the 0.5° × 0.5° grid scale.

Table 1. Comparison of results from high-and low-resolution SSM/I datasets.

	Rainy Pixels #		Total Pixels #		Percentage of Rainy Pixels		Avg. Rainrate of Rainy Pixels (mm h^{-1})			Avg. Rainrate of Total Pixels (mm h^{-1})		
	H	L	H	L	H (%)	L (%)	H	L	L/H Ratio	H	L	H/L Ratio
Cruise 1	4645	1247	109996	27622	4.2	4.5	1.851	2.591	1.40	0.008	0.117	1.50
Cruise 2	15522	4059	121255	30235	12.8	13.4	2.194	2.850	1.30	0.282	0.383	1.36
Cruise 3	10535	2820	120577	30344	8.7	9.3	2.121	2.781	1.31	0.185	0.258	1.39
All Cruises	30702	8126	351828	88201	8.7	9.3	2.117	2.786	1.32	0.185	0.257	1.39

Note: H: high-resolution (deconvolution) SSM/I data. L: Low-resolution (convolution) SSM/I data.

Both version 1 and 2 radar rain datasets are utilized in this paper in order to identify the discrepancies of rainrates from SSM/I retrievals and radar estimations, and to physically explain the systematical bias between rain estimates from SSM/I and shipboard radar measurements.

3. Beam filling issue

Since the deconvolution scheme increases the spatial resolution of the SSM/I observations, rain retrievals based on the deconvolved TBs would lead to more obvious boundaries between raining and non-rainy areas. The beam filling problem is less pronounced with a higher resolution of FOV in satellite microwave-based rain retrievals. We would like to discuss the beam filling issue of satellite microwave-based rain retrievals by studying differences of rain estimates from the high- and low-resolution SSM/I against the shipboard radar measurements. Compared with result from the convolved SSM/I, the horizontal distribution of rainrates from the deconvolved SSM/I reveals more detailed rain structures. Figure 3 shows the time series of maximum rainrates from convolved and deconvolved SSM/I for each overpass over TOGA COARE IFA during IOP. The consistency of the two rain time series is obvious except that the magnitudes of the rainrates at times of large rainfall are much stronger from the deconvolved SSM/I than from the convolved SSM/I. These findings are expected because the deconvolution scheme should better identify strong convection cells due to its fine horizontal resolution.

Table 1 presents comparisons of samples of rainy pixels and total pixels, coverage of rainy pixels, averaged rainrates over rainy pixels and total pixels from deconvolved and convolved SSM/I. It can be seen that the rainy coverage is similar for both high- and low-resolution SSM/I. The lowest rainy coverage and the smallest rainrate are in cruise 1, while the highest rainrate and large rainy coverage are in cruise 2. The averaged rainrates from the convolution scheme are about

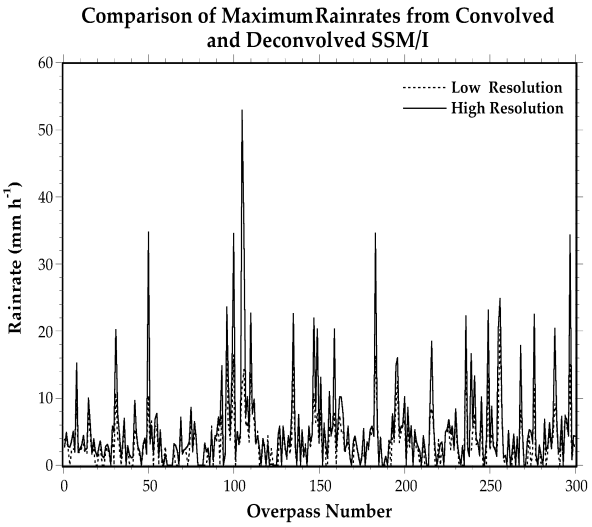

Fig. 3. Comparison of maximum rainrates of each overpass over TOGA COARE IFA for convolved and deconvolved SSM/I.

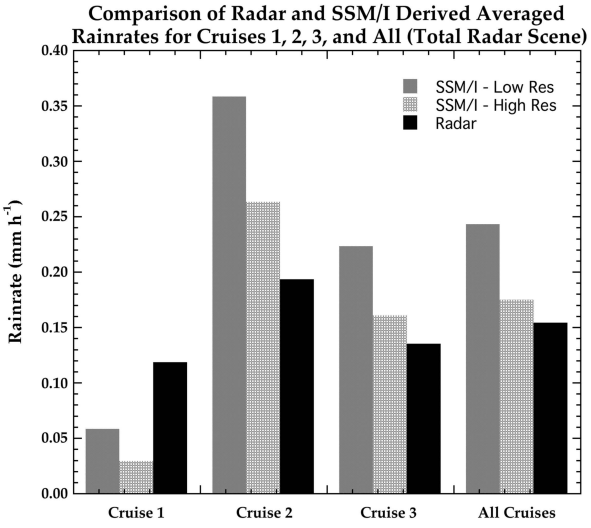

Fig. 4. Bar graphs of mean rainrates from radar and SSM/I measurements for Cruises 1, 2, 3, and All over the total radar scene.

Table 2. Histogram of rainrates from high-and low-resolution SSM/I datasets.

Rainrate<1			1⩽Rainrate<6			6⩽Rainrate		
H(%)	L(%)	L/H Ratio	H(%)	L(%)	L/H Ratio	H(%)	L(%)	L/H Ratio
93.27	90.39	0.97	6.34	9.26	1.46	0.39	0.35	0.90

30%–40% higher than those from the deconvolution scheme for individual cruises and all cruises combined. The rainrate differences between the low- and high-resolution datasets are induced by the nonlinear relationship of rainrates and TBs due to the beam-filling problem. This phenomenon is further explained with the histogram of rainrates derived from the deconvolved and convolved SSM/I datasets (see Table 2). It is evident that there are relatively a few more pixels for small and large rainrates in the decovolution scheme; however, pixels with moderate rainrates increase by about 50% from the high- to low- resolution scheme. The combined impact leads to a higher mean rainrate from the convolution scheme.

Figure 4 shows that the mean rainrates from deconvolved/convolved SSM/I and those from radar measurements have a similar pattern of variations for individual cruises and all cruises combined, although mean rainrates derived from SSM/I are generally higher than those from radar. It is also apparent that discrepancies between rainrates from radar and those from high resolution SSM/I are much smaller than those from radar and low resolution SSM/I. Results indicate that deconvolved SSM/I will overall lead to a better performance in retrieving oceanic precipitation. However, rain retrievals from high resolution SSM/I do not show any improvement in cruise 1. This exception is probably due to the fact that the horizontal scale of the deconvolved SSM/I is still too large for very small-scale rain systems so that the beam filling effect could not be reduced in cruise 1 when weak rain systems dominated. In addition, the relative error of rain retrievals from satellite microwave observations is large for weak rainfall situations (see, Olson et al, 2005). As a result, higher uncertainties of rain estimates from SSM/I exist in cruise 1. The large rain retrieval error for weak systems requires further investigations in current TRMM and future GPM studies.

4. SSM/I-radar rainrate discrepancies

Many validation projects have been conducted to assess rainrates derived from satellite measurements in the past (e.g., PIP-1, PIP-2, PIP-3, AIP-1, AIP-2 and AIP-3). The FSU SSM/I rain retrieval algorithm has performed well in these previous studies (e.g., Barrett et al., 1994; Wilheit et al., 1994; Ebert et al., 1996; Yang and Smith, 1999a). Figure 5a shows the time series of daily rainrates from the radar and the high resolution SSM/I over the TOGA COARE IFA. It is clearly seen that temporal variations of daily rainrates are consistent with each other except during the time periods in which the radar data were missing. Four key statistical parameters are given in the upper left corner. The bias is the difference between the mean rainrates from SSM/I and the radar while the rms is for the root mean square error of the rainrate differences. The ratio of the average daily rainrates from

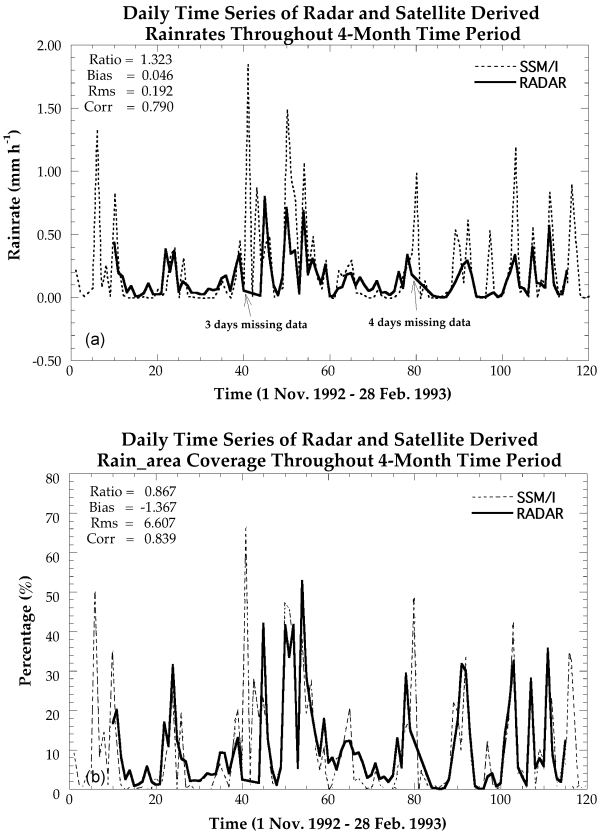

Fig. 5. (a) Daily time series of the version 1 radar rainrates and the deconvolved SSM/I rainrates over TOGA COARE IFA throughout a 4-month time period. (b) For the rainy area coverage.

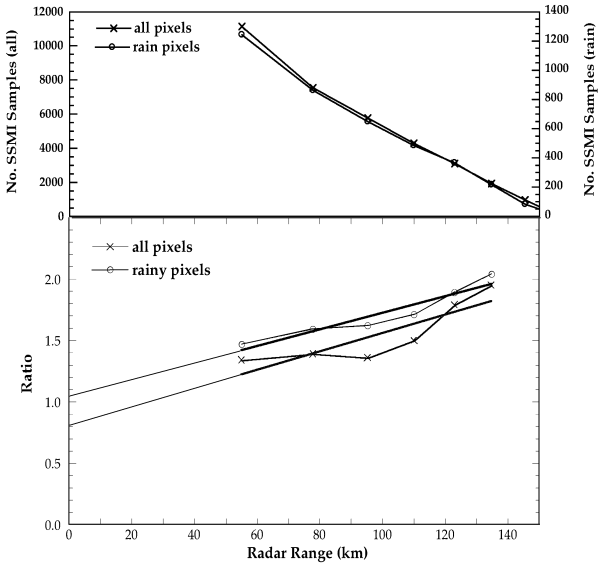

Fig. 6. Radar-range-dependent distributions of SSM/I pixels and the ratio between deconvolved SSM/I-derived rainrates and version 1 radar rainrates for all cruises combined in situations of raining-only pixels and total pixels.

SSM/I and the radar is 1.32, while the bias, rms and correlation coefficient are 0.046, 0.192, and 0.79, respectively.

Figure 5b is the same as Fig. 5a except for the rainy-area coverage. It is obvious that the temporal variations of the daily rainy-area coverage from SSM/I and the radar are very similar. The bias, rms and correlation coefficient are −1.367, 6.607 and 0.84, respectively. The averaged daily rain coverage from SSM/I is less than that from the radar with a ratio of 0.867. It is also known from Fig. 5 that rain systems were inactive during the period of cruise 1 and active during the period of cruise 2. Therefore, Fig. 5 demonstrates that the FSU SSM/I rain retrieval algorithm has the ability to estimate oceanic rainrates, in terms of precipitation intensity, spatial distribution, and temporal variation.

Horizontal distributions of average radar rainfall for individual cruises and all cruises combined indicate that rainfall around the right bottom corner of the IFA area is not reliable due to the small number of radar samples collected when the ships, on which the radars were located, were entering into and departing from the IFA area (figure omitted). Rainrates in cruise 1 were much smaller compared to those in cruise 2 because of the dominance of inactive convection systems in cruise 1 and active convection systems in cruise 2. The maximum rainfall in cruise 1 was located to the southwest of the radar. The maximum rainfall was to the northeast of the radar and decreased gradually toward the southwest in cruise 3. The horizontal distributions of average rainfall for cruise 2 and all cruises combined were similar, indicating a maximum at the center of the radar coverage and the magnitude of the rainfall decreased gradually toward the outside.

Results have shown that the rainrates derived from SSM/I and the radar measurements are consistent, however, their differences are obvious. The question now is whether we can explain these differences. We first examine the variation of the ratio between SSM/I and radar rainrates with distance from the radar. The radar coverage is divided into several concentric zones so that each zone has the same area coverage, then rainrates from SSM/I and the radar located in each zone are separately averaged to represent mean rainrates from SSM/I and the radar for each zone. The bottom panel of Fig. 6 shows the radar-range-dependent ratio variations of average rainrates from SSM/I and the radar for rainy pixels and all pixels. The upper panel gives SSM/I samples of rainy pixels and total pixels applied in the averaging processes in each zone. It is evident that there are sufficient SSM/I pixels in the averaging processes so that the average rainrates from SSM/I are reliable in each zone except for the outermost zone where small samples could not lead to reliable mean rainrates. It can be seen from Fig. 6 that rainrates from SSM/I are greater than those from the radar measurements, and their ratio increases when the distance from a zone to the radar site increases. Distributions of the ratios with radar range are well organized and fit well onto a straight line. The heavy lines in the lower panel are linear regressions of the ratios with radar range over all and rain-only pixels, respectively. The thin lines are the extensions of these regressions. It is evident that the intercepts of the regressions at the radar site for all and rain-only SSM/I pixels are 0.81 and 1.05, respectively. These results suggest that rainrates from SSM/I and the radar measurements are in a very good agreement at the radar site when the radar-range-dependent attenuation is not a factor in the radar rain estimates, although rainrates from SSM/I are much higher than those from the radar measurements and their ratio is proportional to the distance from the radar site. It should also be pointed out that the ratio in the exterior zone is excluded during the regression processes because the small number of samples of SSM/I measurements could lead to a large uncertainty in the average rain retrieval, giving a large error in the ratio. However, similar features still exist even though the ratio in the outside zone is considered. Based on a comparison study of rain gauge and radar-estimated water depth in 65 gauge locations for a shower situation measured by the National Severe Storms Laboratory's WSR-57 radar located in Central Oklahoma, Brande and Sirmans (1976) demonstrated that rainfall

Table 3. Satellite and radar pixel sample counts for three distance-dependent stratifications (both Rain-Only and All categories are considered).

Radius	Equal Area				Equal Radius				Equal Sampling			
	Sat		Radar		Sat		Radar		Sat		Radar	
(EA/ER/ES)	RO	All	RO	All	RO	All	RO	All	RO	All	RO	All
–/15/–	–	–	–	–	63	530	7251	55835	–	–	–	–
–/30/–	–	–	–	–	152	1427	20945	169060	–	–	–	–
–/45/–	–	–	–	–	267	2369	34239	282970	–	–	–	–
55/60/55	1242	11144	102980	841540	361	3249	48936	392420	1498	13486	106990	872920
78/75/75	864	7547	104700	797300	513	4234	66702	507270	1323	11602	98375	751200
95/90/90	650	5766	103780	773540	591	5173	83298	619680	1270	11032	96248	715040
110/105/105	486	4284	97292	753590	712	6082	95160	731290	1499	13010	109930	843500
123/120/120	367	3109	91645	736800	807	7038	106870	842410	1729	15093	123080	971930
135/135/130	219	1933	85585	721730	894	7928	113360	953250	1278	11098	85752	719120
145/–/140	85	972	80431	708590	–	–	–	–	1350	11973	90801	776180

Notations: · EA/ER/ES stand for equal area, equal range, and equal sampling
· RO/All stand for rain only and all pixels

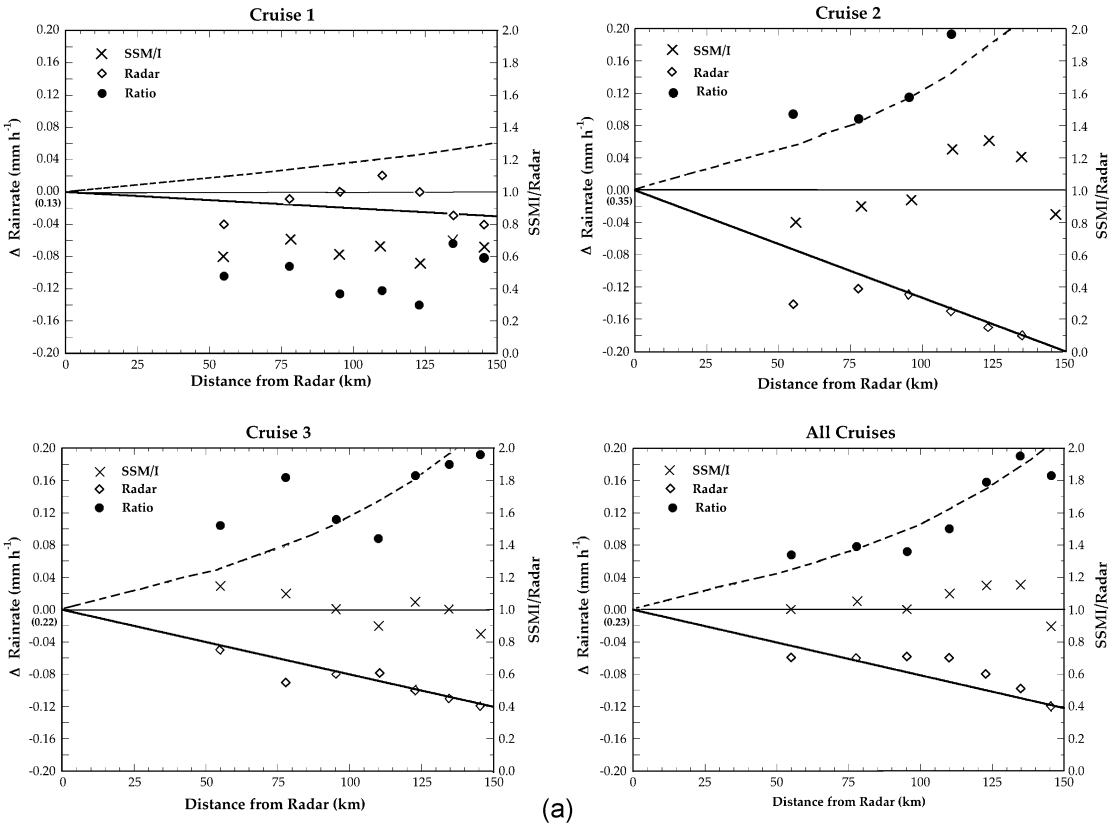

Fig. 7. (a) Range-dependent distributions of deconvolved SSM/I rainrates and version 1 radar rainrates, and their ratio with all radar and SSM/I sampling for Cruises 1, 2, 3, and all cruises combined. (b) for rain-only sampling.

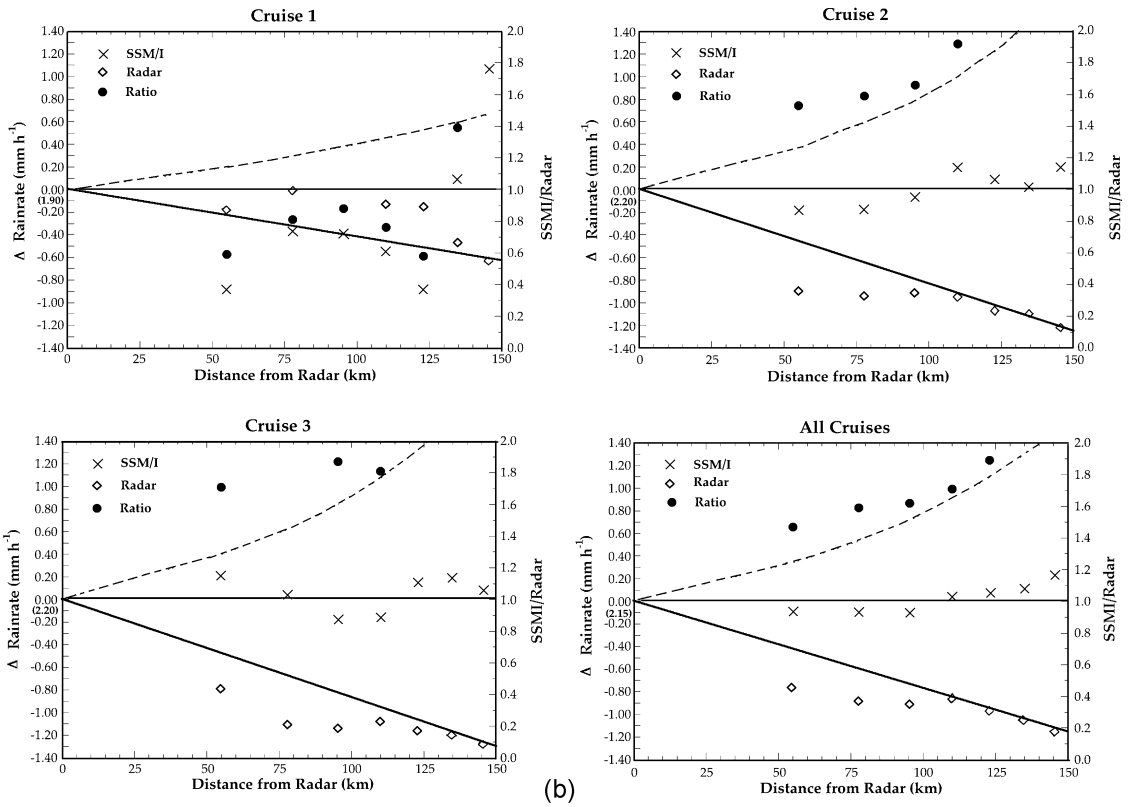

Fig. 7. (Continued).

Table 4. Zero-range intercepts of satellite-radar ratio for three distance-dependent stratifications based on the FSU High resolution algorithm.

	All Pixels	Raining Pixels
Equal Area	0.81	1.05
Equal Radius	0.95	1.09
Equal Sampling	1.02	1.18

measurements from gauges were higher than those from radar, and their ratio increased with the increase of distance from radar site.

In order to demonstrate the credibility of the above results, sensitivity tests are conducted for different selections of the concentric zones. Test I divides the radar scene into several concentric zones so that each zone has nearly equal numbers of SSM/I samples. Test II sets up the concentric zones so that they all have an equal radius. Table 3 presents SSM/I and radar pixels for the three different sorting processes. It can be seen that the distributions of SSM/I samples for situations of equal radius and equal sampling are different from those of equal area, however, the variations of their ratios with radar range are similar to each other (figure omitted). All intercepts of the fitting lines for the three different concentric zones with equal area, equal radius, and equal sampling are summarized in Table 4. Although the intercepts vary with the different approaches, their deviations are small. The composite intercepts for all and rain-only pixels are close to 1 with an overall mean of 1.02 for the three different selections. Results further demonstrate that there is a systematic radar-range-dependent bias in the ratio of rainrates from SSM/I and the radar observations. Since satellite-based rain retrievals are not impacted by the radar range, the systematic bias should mainly be caused by the radar rain estimates.

5. Influences of radar-range-dependent attenuation

The results in section 4 indicate that the overall ratio of rainrates from SSM/I and radar increases with the increase of radar range due to the range-dependent attenuation on radar rain estimates. We now examine the hypothesis that the satellite microwave-based rain

retrievals are reliable while the shipboard radar rain estimates are correctable. This hypothesis is based on two reasonable assumptions: (1) rainrates from both SSM/I and the radar observations are accurate at the radar location; and (2) rainrates from SSM/I do not vary with radar range, in conjunction with the well-known fact that rainrates from C-band or higher-frequency radar are strongly associated with a range-dependent attenuation. Therefore, the maximum rainrate estimate occurs at the radar site, where the ratio of rainrates from SSM/I and the radar is 1.

Figure 7 is applied to determine the credibility of the above hypothesis. This figure shows rainrates from the high resolution SSM/I and the radar in different concentric zones with equal area for individual cruises and all cruises combined, the variation of their ratios with radar range, and the hypothesized radar rainrates and ratio variation for all pixels and rainy pixels, respectively. The left y-axis shows the differences between rainrates in a concentric zone and at the radar location. The right y-axis is the ratio of rainrates from SSM/I and the radar. The value in parentheses is the hypothesized rainrate at the radar site. The x-axis is the radar range. The thin straight line, which is the distribution of hypothesized rainrates, does not vary with radar range. The heavy straight line is the hypothesized rainrate from the radar. The dashed line is the ratio distribution of the hypothesized rainrate from SSM/I and the radar.

Figure 7a is for all pixels. It is evident that for the all cruises-combined situation both estimated rainrates from SSM/I and the radar agree well with the hypothesized distributions, respectively. In addition, the distribution of the hypothesized ratios fits well with the measured ratios. These features are also apparent for cruises 2 and 3. However, they are not seen in cruise 1. Similar features exist for the rainy pixel situation (Fig. 7b).

Why does this hypothesis not bode well for cruise 1 while it is generally robust for cruises 2 and 3 and for all cruises combined? We have to use various weather conditions during these cruises to understand why cruise 1 is an exception. Rainy weather systems were inactive with only about 4.2% rain coverage from the SSM/I measurements during cruise 1 and their overall rainfall was small. The inactive weather systems during cruise 1 led to small numbers of rainy SSM/I samples which in turn generated more errors in the satellite rain retrievals. The most important factor of the weak rainfall activities during cruise 1 was that failures of detecting some small rainfall events were inevitable because of the beam-filling issue in the SSM/I measurements.

Nevertheless, the results demonstrate that the ratio increase with radar range between rainrates from SSM/I and the radar is mainly caused by the rainrate decrease with radar range from the radar measurements. Since the measured rainrates from SSM/I and the radar in Fig. 7 do not perfectly match the hypothesized rainrates, there must be more reasons to explain their discrepancies in addition to the radar-range-dependent attenuation. First, radar rainrates based on $Z-R$ relationships depend on the amplitudes of reflectivity detected by the radar receiver. The attenuation effect of radar reflectivity on rain estimates typically results in the estimated rainfall being smaller than the true values. The attenuation effect is proportional to the distance from the rain clouds to the radar site such that the effect becomes stronger when the distance increases. The attenuation effect is also proportional to the rain intensity so that there is a greater attenuation effect on heavy rainfall. These features can be seen from Figs. 4 and 7 for cruise 2. The difference in the rainfall from SSM/I and the radar is the largest in cruise 2 because there were more heavy rainfall activities in cruise 2 than in the other cruises. The attenuation impact is also the strongest in cruise 2 while it is the weakest in cruise 1. Brande and Sirmans (1976) pointed out that the discrepancy of gauge versus radar rainfall became much smaller when the radar measurements are corrected for attenuation effects. Second, the importance of selecting an appropriate $Z-R$ relationship in the radar rain estimates is obvious. In addition, since Doppler radar is operated at a fixed elevation angle and beam width, the radar can possibly detect areas above the rain clouds or part of the rain clouds when the clouds are far away from the radar site (i.e., the radar cloud top overshooting problem). Thus, radar reflectivity at those distances does not adequately reflect the real rain systems, thus leading to rain underestimation. Furthermore, incomplete radar beam filling also leads to underestimated rainrates. In addition, vertical velocity, which changes the vertical rain-water flux and hence changes the drop-size distribution in vertically inhomogeneous situations, can induce errors in the Z-R relationships (Carbone and Nelson, 1978). Finally, proper radar calibration is the most important issue in rain estimates from ground

radar measurements.

Any one or combined factors discussed above may have led to the serious underestimations of the version 1 radar rain datasets over the TOGA COARE IFA. The version 2 radar rain datasets were released later with different $Z - R$ relationships and new calibrations (Short et al., 1997). Comparisons of rainrates from SSM/I rain retrieval algorithms and the version 2 radar dataset are much better with respect to the version 1 radar dataset [see Ebert and Manton (1998) for detailed intercomparison results]. Figure 8 shows the comparison of the high resolution SSM/I rainfall and the version 2 radar rainfall. It is evident that both ratios of rainrates from SSM/I and the radar for all pixels and rainy pixels do not significantly increase with radar range. Their linear regression lines are almost flat with intercepts of 1.01 and 1.19, respectively at the zero radar range. These results further demonstrate that the quality of the AIP-3 v2 ground radar-based rainrates has been significantly improved while the high-resolution satellite microwave-based rain retrievals are reliable so that a higher consistency between the satellite microwave-based rainrates and the improved radar rain estimates is expected, although small differences still exist.

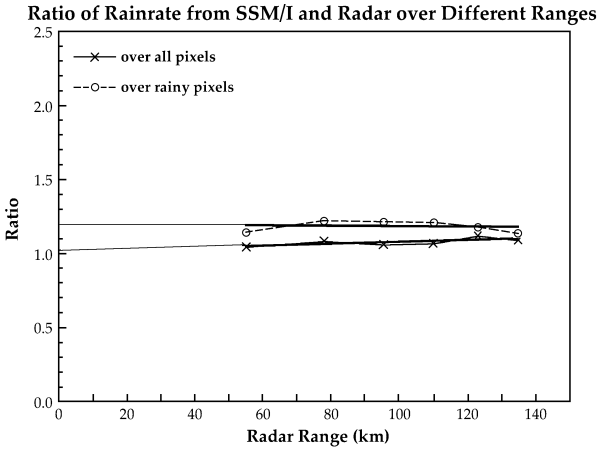

Fig. 8. Same as Fig. 6, except for version 2 radar rain data with a range adjustment.

6. Discussion and conclusions

Analysis of rainrates from SSM/I retrievals and radar measurements has been performed for AIP-3 over the TOGA COARE IFA. The original SSM/I measurements used in rainrate retrieval processes have been arranged in two different datasets, viz., the high- and low- resolution SSM/I datasets. The high-resolution (i.e., deconvolution) SSM/I data are processed so that the low-frequency channels are enhanced to the resolution of the 85-GHz channel. The low-resolution (i.e., convolution) data are organized so that the 85-GHz channel is weight-averaged to the 37-GHz channel resolution. Comparison of rainrates from the high- and low-resolution SSM/I datasets shows that their horizontal distribution patterns are similar, as expected. However, the high- resolution rainrates reveal more detailed rain structures than the low-resolution rainrates because the spatial scales of rain cells are often smaller than the footprints of the low frequency SSM/I channels. The spatially-temporally averaged rainrate from the convolved SSM/I is about 30%-40% higher than that from the deconvolved SSM/I because the non-homogeneous beam-filling problem in the low-resolution dataset leads to a 50% increase of rainy pixels for moderate intensities of the rainrate with respect to the high-resolution SSM/I data. Comparison results of rainrates from the high- and low-resolution SSM/I and the radar indicate that the deconvolution scheme can lead to better precipitation estimates from SSM/I measurements.

This study shows that the deconvolution scheme improves the accuracy of rain estimates by 28% from the SSM/I measurements. The overall intercept at the radar location of the ratio between the high-resolution SSM/I and radar rainrates is 1.02, indicating that the radar estimates of the rainrates are close to the SSM/I rain retrievals at the radar site. It is also evident that the radar rainrates are underestimated far from the radar location due to the effects of range-dependent attenuation and incomplete beam filling from the radar measurements.

The version 1 and 2 radar rain datasets have been utilized to demonstrate the hypothesis that SSM/I-based rain retrievals are reliable while ship-based radar rain estimates are correctable. We provide evidence that there is a systematic difference between the satellite retrievals and the version 1 radar estimates of rainrates over the IFA area with an outstanding range-dependent bias in the radar rainrates. Two reasonable assumptions were associated with this hypothesis, viz., both radar and satellite estimates of the rainrates are right at the radar site, and the satellite rain retrievals do not vary with radar range, in addition to the fact that a range-dependent attenuation exists with the AIP-3 radar rainrates. The results

show that the hypothesized range-dependent distributions of rainrates from satellite and ship-borne radar measurements and their ratio are generally consistent with the observed distributions for cruises 2 and 3, and all cruises-combined. It demonstrates that the hypothesis is believable. With the version 2 radar rain datasets, the ratio of rainrates from satellite and radar does not vary significantly with radar range for all cruises-combined, with values of about 1.01 and 1.2 for all pixels and rainy pixels, respectively. These results further support the robustness of the hypothesis. However, this hypothesis is not solid during the time period of cruise 1 when weak rain activities were dominant. The smaller impact of range-dependent attenuation on weak rainfall and the greater uncertainty in small rainfall measuraments from SSM/I retrievals can partially explain this feature for cruise 1. The results also suggest that more investigations are needed to further explain the discrepancies between rainrates estimated from satellite microwave instruments and from ground-radar measurements.

Nevertheless, evidence shows that satellite microwave-derived rainfall can be used to evaluate rain estimates from ground-based observations and numerical model simulations. It also suggests that the effects of the range-dependent attenuation on ground radar rain estimates have to be carefully studied in validating TRMM and GPM satellite-based rain retrievals when the ground radar rainrates are used as the "truth".

Acknowledgments. The authors would like to thank Dr. David A. Short at NASA/GSFC and Dr. Elizabeth E. Ebert at the Bureau of Meteorology Research Centre in Melbourne, Australia for discussions on the AIP-3 rainfall intercomparison project. They also appreciate the two anonymous reviewers for their comments that significantly improved the quality of this paper. This study was supported by the NASA Global Precipitation Measurement Project.

REFERENCES

Adler, R. F., and A. J. Negri, 1988: A satellite infrared technique to estimate tropical convective and stratiform rainfall. *J. Appl. Meteor.*, **27**, 30–51.

Adler, R. F., A. J. Negri, P. R. Keehn, and I. M. Hakkarinen, 1993: Estimation of monthly rainfall over Japan and sounding waters from a combination of low-orbit microwave and geosynchronous IR data. *J. Appl. Meteor.*, **32**, 335–356.

Adler, R. F., G. J. Huffman, D. T. Bolvin, S. Curtis, and E. J. Nelkin, 2000: Tropical rainfall distributions determined using TRMM combined with other satellite and rain gauge information. *J. Appl. Meteor.*, **39**, 2007–2023.

Adler, R. F., C. Kidd, G. Petty, M. Morissey, and H. M. Goodman, 2001: Intercomparison of global precipitation products: The Third Precipitation Intercomparison Project (PIP-3). *Bull. Amer. Meteor. Soc.*, **7**, 1377–1396.

Arkin, P. A., 1979: The relationship between fractional coverage of high cloud and rainfall accumulations during GATE over the B-scale array. *Mon. Wea. Rev.*, **107**, 1382–1387.

Arkin, P. A., and B. N. Meisner, 1987: The relationship between large-scale convective rainfall and cold cloud over the western hemisphere during 1982–84. *Mon. Wea. Rev.*, **115**, 51–74.

Arkin, P. A., and P. Xie, 1994: The global Precipitation Climatology Project: First Algorithm Intercomparison Project. *Bull. Amer. Meteor. Soc.*, **75**, 401–419.

Atlas, D., D. Rosenfeld, and D. A. Short, 1990: The estimation of convective rainfall by area integral. Part I. The theoretical and empirical basis. *J. Geophys. Res.*, **95**, 2153–2160.

Barrett, E. C., and Coauthors, 1994: The first WetNet Precipitation Intercomparison Project (PIP-1): Intercompasion of results. *Remote Sensing Review*, **11**, 303–373.

Brandes, E., and D. Sirmans, 1976: Convective rainfall estimation by radar: Experimental results and proposed operational analysis technique. Preprints, *Conf. Hydro-meteorol.. 1976*, 54–59.

Carbone, R. E., and L. D. Nelson, 1978: The evolution of raindrop spectra in warm-based convective storms as observed and numerically modeled. *J. Atmos. Sci.*, **35**, 2302–2314.

Ebert, E. E., M. J. Manton, P. A. Arkin, R. J. Allam, G. E. Holpin, and A. Gruber, 1996: Results from the GPCP algorithm intercomparison programme. *Bull. Amer. Meteor. Soc.*, **77**, 2875–2887.

Ebert, E. E., and M. J. Manton, 1998: Performance of satellite rainfall estimation algorithms during TOGA COARE. *J. Atmos. Sci.*, **55**, 1537–1557.

Farrar, M. R., and E. A. Smith, 1992: Spatial resolution enhancement of terrestrial features using deconvolved SSM/I microwave brightness temperature. *IEEE Trans. Geosci. Remote Sens.*, **30**, 349–355.

Farrar, M. R., E. A. Smith, and X. Xiang, 1994: The impact of spatial resolution enhancement of SSM/I microwave brightness temperature on rainfall retrieval algorithms. *J. Appl. Meteor.*, **33**, 313–333.

Haddad, Z. S., E. A. Smith, C. D. Kummerow, T. Iguchi, M. R. Farrar, S. L. Durden, M. Alves, and W. S. Olson, 1997: The TRMM "Day-1" radar/radiometer combined rain-profiling algorithm. *J. Meteor. Soc. Japan*, **75**, 799–809.

Hinton, B. B., W. S. Olson, D. W. Martin, and B. Auvine, 1992: A passive microwave algorithm for tropical oceanic rainfall. *J. Appl. Meteor.*, **31**, 1379–1395.

Iguchi, T., T. Kozu, R. Meneghini, J. Awaka, and K. Okamoto, 2000: Rain-profiling algorithm for the TRMM precipitation radar. *J. Appl. Meteor.*, **39**, 2038–2052.

Kummerow, C., R. A. Mack, and I. M. Hakkarinen, 1989: A self-consistency approach to improve microwave rainfall estimates from space. *J. Appl. Meteor.*, **28**, 869–884.

Kummerowc., I. M. Hakkarinen, H. F. Pierce, and J. A. Weinman, 1991: Determination of precipitation profiles from airborne passive microwave radiometric measurements. *J. Atmos. Oceanic Technol.*, **8**, 148–158.

Kummerow, C., and Coauthors, 2001: The evolution of the Goddard profile algorithm (GPROF) for rainfall estimation from passive microwave sensors. *J. Appl. Meteor.*, **40**, 1801–1820.

Mugnai, A., H. J. Cooper, E. A. Smith, and G. J. Tripoli, 1990: Simulation of microwave brightness temperature of an evolving hailstorm at SSM/I frequencies. *Bull. Amer. Meteor. Soc.*, **71**, 2–13.

Mugnai, A., E. A. Smith, and G. J. Tripoli, 1993: Foundations for statistical–physical precipitation retrieval from passive microwave satellite measurements. Part II: Emission-source and generalized weighting-function properties of a time-dependent cloud-radiation model. *J. Appl. Meteor.*, **32**, 17–39.

Olson, W. S., and Coauthors, 2005: Precipitation and latent heating distributions from satellite passive microwave radiometry. Part I: Method and uncertainties. *J. Appl. Meteor.* (in press).

Short, D. A., and G. R. North, 1990: The beam filling error in the Nimbus 5 Electrically Scanning Microwave Radiometer observations of Global Atlantic Tropical Experiment rainfall. *J. Geophys. Res.*, **95**, 2187–2193.

Short, D. A., P. A. Kucera, B. S. Ferrier, J. C. Gerlach, S. A. Rutledge, and O. W. Thiele, 1997: Shipboard radar rainfall patterns within the TOGA COARE IFA. *Bull. Amer. Meteor. Soc.*, **78**, 2817–2836.

Simpson, J., C. Kummerow, W.-K. Tao, and R. Adler, 1996: On the Tropical Rainfall Measuring Mission (TRMM). *Meteorology and Atmospheric Physics*, **60**, 19–36.

Smith, E. A., and S. Q. Kidder, 1978: A multispectral satellite approach to rainfall estimates. Tech. Rep., Department of Atmospheric Sciences, Colorado State University, Ft. Collins, CO, 49pp.

Smith, E. A., A. Mugnai, H. J. Cooper, G. J. Tripoli, and X. Xiang, 1992: Foundations for statistical–physical precipitation retrieval from passive microwave satellite measurements. Part I: Brightness temperature properties of a time dependent cloud–radiation model. *J. Appl. Meteor.*, **31**, 506–531.

Smith, E. A., C. Kummerow, and A. Mugnai, 1994a: The emergence of inversion-type precipitation profile algorithms for estimation of precipitation from satellite microwave measurements. *Remote Sensing Reviews*, **11**, 211–242.

Smith, E. A., X. Xiang, A. Mugnai, R. E. Hood and R. W. Spencer, 1994b: Behavior of an inversion-based precipitation retrieval algorithm with high resolution AMPR measurements including a low frequency 10.7 GHz channel. *J. Atmos. Oceanic Technol.*, **11**, 858–872.

Smith, E. A., X. Xiang, A. Mugnai, and G. Tripoli, 1994c: Design of an inversion-based precipitation profile retrieval algorithm using an explicit cloud model for initial guess microphysics. *Meteorlogy and Atmospheric Physics*, **54**, 53–78.

Smith, E. A., and Coauthors, 1998: Results of WetNet PIP-2 project. *J. Atmos. Sci.*, **55**, 1483–1536.

Spencer, R. W., H. M. Goodman, and R. E. Hood, 1989: Precipitation retrieval over land and ocean with SSM/I : Identification and characteristics of the scattering signal. *J. Atmos. Oceanic Technol*, **6**, 254–273.

Wilheit, T. T., and Coauthors, 1994: Algorithms for the retrieval of rainfall from passive microwave measurements. *Remote Sensing Review*, **11**, 163–194.

Wilheit, T. T., A. T. C. Chang, M. S. V. Rao, E. B. Rodgers, and J. S. Theon, 1977: A satellite technique for quantitatively mapping rainfall rates over the ocean. *J. Appl. Meteor.*, **16**, 551–560.

Yang, S., 2004: Precipitation and latent heating estimation from passive microwave satellite measurements: A review. *Observations, Theory, and Modeling of the Atmospheric and Oceanic Variability*. World Scientific Series on Meteorology of East Asia, Vol. 3, World Scientific Publishing Co. Pte. Ltd., Singapore, 484–500.

Yang, S., and E. A. Smith, 1999a: Moisture budget analysis of TOGA-COARE using SSM/I retrieved latent heating and large scale Q_2 estimates. *J. Atmos. Oceanic Technol.*, **16**, 633–655.

Yang, S., and E. A. Smith, 1999b: Four dimensional structure of monthly latent heating derived from SSM/I satellite measurements. *J. Climate*, **12**, 1016–1037.

Yang, S., and E. A. Smith, 2000: Vertical Structure and transient behavior of convective-stratiform heating in TOGA COARE from combined satellite-sounding analysis. *J. Appl. Meteor.*, **39**, 1491–1513.

Yang, S., W. S. Olson, J.-J. Wang, T. L. Bell, E. A. Smith, and C. D. Kummerow, 2005: Precipitation and latent heating distributions from satellite passive microwave radiometry. Part II: Evaluation of estimates using independent data. *J. Appl. Meteor.* (in press).